

Beyond “fire temperatures”: calibrating thermocouple probes and modeling their response to surface fires in hardwood fuels

Anthony S. Bova and Matthew B. Dickinson

Abstract: The maximum temperatures of thermocouples, temperature-sensitive paints, and calorimeters exposed to flames in wildland fires are often called “fire temperatures” but are determined as much by the properties and deployment of the measurement devices as by the fires themselves. Rather than report device temperatures that are not generally comparable among studies, we show that maximum and time-integrated temperatures of relatively thick (4.8 mm diameter) type-K thermocouple probes (TCPs) can be calibrated to estimate fuel consumption and fire line intensity in surface fires. Although reporting standard fire characteristics is an improvement over reporting device temperatures, TCPs are not ideal instruments for monitoring surface fires, because they provide only point estimates of fire behavior and must be calibrated for different fire environments, TCP characteristics, and deployments. To illustrate how TCPs respond to fires and to point the way towards a more general calibration method, we report results from a numerical model that accurately simulated TCP response to a spreading surface fire.

Résumé : La température maximale des thermocouples, des peintures thermosensibles et des calorimètres exposés aux flammes produites par les feux de forêt est souvent appelée « température du feu » mais elle est déterminée aussi bien par les propriétés et la façon dont sont utilisés ces appareils de mesure que par les feux eux-mêmes. Plutôt que de rapporter la température mesurée par des appareils, laquelle n'est généralement pas comparable d'une étude à l'autre, nous montrons que la température maximale et la température intégrée dans le temps des sondes relativement épaisses (4,8 mm de diamètre) des thermocouples de type K (STCs) peuvent être calibrées pour estimer la consommation de combustibles et l'intensité de la ligne de feu dans le cas des feux de surface. Bien que le fait de rapporter des caractéristiques standards du feu plutôt que la température mesurée par des appareils constitue une amélioration, les STCs ne sont pas les instruments idéaux pour assurer le suivi des feux de surface parce qu'ils fournissent seulement des estimations ponctuelles du comportement du feu et qu'ils doivent être calibrés pour différents environnements, différentes caractéristiques des STCs et différentes façons de les utiliser. Pour illustrer comment les STCs réagissent aux feux et ouvrir la voie vers une méthode de calibration plus générale, nous rapportons les résultats d'un modèle numérique qui simule avec exactitude la réaction des STCs à un feu de surface qui se propage.

[Traduit par la Rédaction]

Introduction

In the ecological and forestry literature on fire effects, it is common to find studies that characterize forest fires using temperature-measurement devices such as thermocouple probes (TCPs), bare thermocouples, temperature-sensitive paint tags, or stirred calorimeters. Device temperatures are often referred to as “fire temperatures,” although they range from 60 °C to >1000 °C (e.g., Bailey and Anderson 1980; Williamson and Black 1981; Archibold et al. 1998; Lippincott 2000; Iverson et al. 2004; Kennard et al. 2005; Wally et al. 2006).

In fact, peak flame temperatures in small wildland fires, such as surface fires, vary over a relatively narrow range, from 800 to about 1200 °C (Van Wagner and Methven

1978; Dupuy et al. 2003), although they may be higher in crown fires (Butler et al. 2004). Temperatures attained by the above devices depend on their thermophysical properties and position relative to the fire, as well as wind and flame velocities, flame temperature, residence time, and fuel consumption. Thus, fire temperatures may vary considerably when measured by different devices exposed to the same fire environment (e.g., Kennard et al. 2005). Obviously, this is a disadvantage when attempts are made to compare studies and understand fire effects (Van Wagner and Methven 1978; Dickinson and Johnson 2001).

In addition, even if the mean temperature of flame gases are accurately estimated in a fire, this is only one of the elements necessary to estimate heat transfer to objects or organisms exposed to surface fires. In other words, temperature by itself is not a particularly useful measure of surface fire characteristics or effects (VanWagner and Methven 1978).

Despite these limitations, such temperature measurement devices are likely to be employed in wildland fire experiments in the future. Although not ideal, TCPs in particular are popular, because they are relatively inexpensive. They are also more portable than calorimeters and, unlike metal

Received 25 May 2007. Accepted 24 October 2007. Published on the NRC Research Press Web site at cjfr.nrc.ca on 25 April 2008.

A.S. Bova¹ and M.B. Dickinson. USDA Forest Service, Northern Research Station, Forestry Sciences Laboratory, 359 Main Road, Delaware, OH 43015-8640, USA.

¹Corresponding author (e-mail: abova@fs.fed.us).

tags coated with temperature sensitive paints, can provide a time series of data. Although they do not indicate true flame temperature, it is clear that TCPs respond to the energy produced by a surface fire. This suggests that it should be possible to calibrate their response by commonly used surface fire characteristics, such as fuel consumption or fire line intensity.

The diversity of factors that influence a TCP in a surface fire, including uncontrollable (in outdoor experiments) environmental variables, makes comprehensive testing difficult. To better illustrate the effects of some of these variables and to explore the possibility of inversely matching TCP response to fire conditions, a simple model of TCP response was constructed using standard heat transfer formulas and semiempirical relations describing flame height and temperature.

In this paper, we present functional calibrations that can be used to estimate fuel consumption and fire line intensity from the temperature history of a type of TCP commonly mounted in surface fires. The calibrations are derived from data obtained from 12 instrumented plot fires in mixed-oak forest litter and woody fuels.

Heat transfer and model components

Relevant principles of heat transfer to a TCP and corresponding components of the model are described below. The model has two distinct parts. Firstly, characteristics of a surface fire, such as flame height and flame velocity, are estimated from fuel consumption and rate of spread. Secondly, resulting radiative and convective heat transfer to a TCP is estimated, based on its prescribed thermophysical properties, as the surface fire moves past it. Data from the plot experiments that were used to partially validate the model are described in the Methods section.

Surface fire

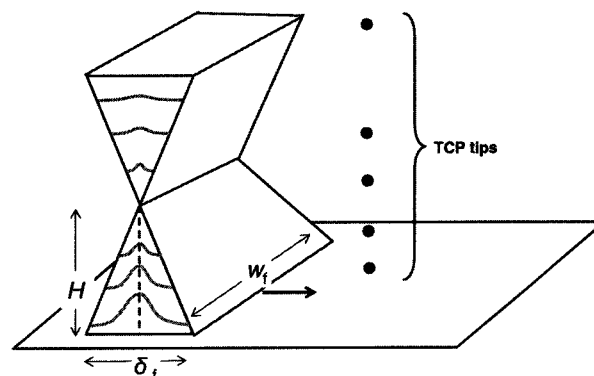
Surface fire was idealized in the model as a triangular prism of centerline height, H (m), width, w_f (m), and base depth, δ_f (m), with a "plume" formed by an inverted triangular prism of equal dimensions (Fig. 1). The practical effect of this is simply to provide, based on flame depth and rate of spread, a flame or plume residence time and temperature profile at the tip of a modeled TCP.

A commonly used correlation for flame length in wildland flames is that found by Byram (from Johnson 1992):

$$[2] \quad \begin{aligned} \Delta T &= T_f - T_o & Z < 0.75 \\ \Delta T &= (T_f - T_o)(Z/0.75)^{-0.86} & 0.75 \leq Z \leq 0.97 \\ \Delta T &= (T_f - T_o)(Z/0.75)^{-0.86}(Z/0.97)^{-2.17} & Z > 0.97 \end{aligned}$$

where $T_f - T_o$ (1040 °C) is maximum excess flame temperature and Z is dimensionless height along the flame centerline (i.e., distance above the fuel surface divided by flame height). Maximum excess flame temperature was corrected for thermocouple radiation error and is close to that found by Walker and Stocks (1968), who estimated mean maximum flame temperature above pine needle fuel beds at 1093 °C.

Fig. 1. Triangular flame and plume prisms used to model thermocouple probe (TCP) response to surface fires. Gaussian temperature profiles are indicated in cross sections. Variation in the height of TCP tips are shown for illustration. H , surface fire centreline height (m); w_f , surface fire width (m); δ_f , surface fire base depth (m).



$$[1] \quad L = \left(\frac{I}{259.83} \right)^{0.46}$$

Fire line intensity, I (kW·m⁻¹), is defined as $I \equiv h_c WR$, where h_c (16 000 kJ·kg⁻¹) is the mean low heat of combustion available to flaming (Nelson 2002), W (kg·m⁻²) is consumed dry fuel loading, and R (m·s⁻¹) is rate of flame spread in the direction of propagation. In the no-wind case, flame length is equal to flame height ($L = H$). Equation 1 gives flame lengths somewhat shorter than the correlations given by Yuan and Cox (1996) and McCaffrey (1979), who were working with rectangular gas burners, and by Dupuy et al. (2003), who used a cylindrical forest fuel burner.

Flame width, w_f , was assigned a value of 4 m in all cases (Fig. 1), although Wotton et al. (1999) noted that thermal radiation from a surface flame to a point in the fuelbed did not increase significantly once flame widths were >2 m. In some of the plot experiments (see Methods section), effective flame width relative to a given TCP was sometimes <2 m; thus, thermal radiation will be overestimated in corresponding simulations.

Flame temperatures above a circular burner of forest fuels (pine needles and excelsior) were estimated by Dupuy et al. (2003) from the temperatures of thin thermocouples. The mean centerline temperature over ambient (i.e., excess temperature), ΔT , may be expressed as a piecewise function (Dupuy et al. 2003):

The conditional statements in eq. 2 distinguish, in order, the continuous, intermittent, and plume regions of a flame. It should be noted that Dupuy et al. (2003) do not recommend this relationship for the region $Z < 0.3$, because flame temperature tends to fall slightly near the fuel surface. Similar results are found in McCaffrey (1979) and Yuan and Cox (1996) for natural gas flames above porous refractory burners. However, because the drop in temperature is small

Table 1. Specific heat correlations for TCP components.

TCP component	Component mass fraction (estimated)	Specific heat as function of temperature (J·kg ⁻¹ ·K ⁻¹)	Source
MgO	0.32	$0.2889 + 2.9 \times 10^{-5} (T - 273) - (6310/T^2)$	Victor and Douglas 1960
304 SS	0.62	$450 + 0.280(T - 273) - 2.91 \times 10^{-4} (T - 273)^2 + 1.34 \times 10^{-7} (T - 273)^3$	Gardner and Ng 2006
Chromel	0.034	$0.1786T + 394.3$	Buttsworth 2001
Alumel	0.034	$0.07512T + 500.8$	Buttsworth 2001

and for the sake of simplicity, we assume $\Delta T = T_f - T_o$ within this region as well.

The cross-sectional temperature profile at a given height within the flame was modeled as a Gaussian function with a maximum at the centerline position of the flame (Dupuy et al. 2003; Quintiere 2006) (Fig. 1). The equation below gives a temperature close to that of ambient at the edge of the flame:

$$[3] \quad T(x, \delta) = T_f \exp \left[- \left(\frac{4x}{\delta(z)} \right)^2 \right]$$

where x (m) is the horizontal position measured from the center (at 0 m) and $\delta(z)$ (m) is the horizontal depth of the flame prism at a given height above the flame base (i.e., the fuel surface) (Fig. 1). This profile simply approximates the temperature of the portion of the flame that is in contact with the modeled TCP as the flame prism moves past it.

An object at uniform temperature, T (K), emits thermal radiation with a total emissive power per unit area, E (W·m⁻²), that is given by the Stefan–Boltzmann law, $E = \sigma \varepsilon T^4$. The constant, σ , has an approximate value of 5.67×10^{-8} W·m⁻²·K⁻⁴. Emissivity, ε , is defined as the ratio of a real body's emissive power to that of an ideal blackbody at the same temperature. By definition, ε is a dimensionless quantity varying from zero to unity.

Modeling the emissive power of a flame is difficult, because flame temperature varies spatially (eqs. 2 and 3) and temporally. The ε of a flame also depends upon soot content and optical thickness (Pastor et al. 2002). As is common in engineering calculations (e.g., Gardner and Ng 2006), we assume that ε is independent of wavelength.

Flame ε may be expressed by the function $\varepsilon = 1 - \exp[-k\delta(z)]$, where k (m⁻¹) is a constant that is found empirically (Drysdale 1998). Pastor et al. (2002) found values of 3.11 and 2.24 for k at one-quarter and three-quarter flame heights, respectively, in vertical flames from wild-land fuels. Fitting these values to a linear equation over dimensionless lengths from zero to unity along the flame centerline gives (adapted from Pastor et al. 2002):

$$[4] \quad \varepsilon(\delta, Z) = 1 - \exp[(1.74Z - 3.55)\delta]$$

Combining this relation with a suitable mean flame temperature, a simple model for mean emissive power, \bar{E} (W·m⁻²), is

$$[5] \quad \bar{E} = \frac{\sigma}{L} \int_0^L \varepsilon(\delta, Z) \bar{T}^4 dz$$

where $\bar{T} = 830$ °C (1100 K), and $\delta = \delta(Z)$ is implied. When eq. 5 is combined with a view factor (eq. 11 below), the

flame is further idealized as a two-dimensional wall of uniform temperature and dimension, $L \cdot w_f$, that moves past the TCP at a constant rate of spread. The accuracy and practicality of this approach, which is used to model only radiative heat transfer, will be discussed further.

An estimate of the velocities of heated gases is required to model the convective heating of a TCP. McCaffrey (1979) notes that the approximate time-averaged centerline velocity throughout all regions (i.e., continuous, intermittent, and plume) of a pool fire is given by

$$[6] \quad u \approx 0.94 \left(\frac{2g\Delta T}{T_o} \right)^{0.5}$$

where u (m·s⁻¹) is vertical velocity, g (9.8 m·s⁻²) is gravitational acceleration, and T_o (K) is ambient temperature. We assume that this relation can also be used for surface line fires, because the same principle of temperature gradient-induced buoyancy applies. The velocity distribution through the depth of the modeled flame was assumed to have the same Gaussian profile as temperature (eq. 3). Gas speed, s (m·s⁻¹), over the probe was modeled as the resultant of (vertical) flame and (horizontal) wind speeds, that is, $s = (u^2 + v^2)^{0.5}$. Flame tilting due to wind was erratic in the plot fires described below. Because of this and for simplicity, flame tilting was not modeled (i.e., flame length = flame height).

TCP thermophysical properties

The cylindrical TCPs used in the small plot experiments described below (see Methods section) have a sheath of polished AISI 304 stainless steel of radius of 2.4 mm (0.6 mm thick) containing an isolated type-K (chromel-alumel) thermocouple hard-packed in magnesium oxide (MgO) powder. TCP bulk density (5700 kg·m⁻³) was estimated from the estimated volumes and known densities of its components. It was assumed that TCP density and radius remain constant throughout heating.

The specific heat of a TCP is temperature dependent and was estimated from empirical correlations for the specific heat of the TCP components weighted by their respective mass fractions (Table 1).

TCP ε is chiefly a function of sheath composition and roughness. Unlike carbon steel, the ε of type 304 steel stays relatively constant from 273 K to 1273 K (Paloposki and Liedquist 2005; Bauer et al. 2003). Gardner and Ng (2006) suggest that ε of structural steel (type 304) exposed to fire be taken as 0.2, although Otsuka et al. (2005) note that the total hemispherical ε of this type of steel may rise from about 0.15 to 0.4 over the temperature range 750 K to 1000 K, owing to a thin oxide layer. However, maximum TCP temperatures in the experiments described below reached only

the lower end of this range; therefore, ε was given a constant value 0.2 in the model. The deposition of flame-generated soot onto a TCP may also affect its ε and absorptivity, but soot was removed from the TCPs before each experiment, and no attempt was made to model its effects.

Wildland fires radiate mostly in the midinfrared through thermal-infrared regions of the spectrum (Briz et al. 2003). In this range, 304 stainless steel absorbs only about 20% of incident radiation (Karlsson and Ribbing 1982); thus, absorptivity was also assigned a value of 0.2 in the model.

TCP response to heat transfer

The temperature indicated by a TCP is that of the thermocouple junction, which is usually located within the probe tip, although it was assumed here to be the temperature of the entire probe assembly near the tip at any instant. This assumption becomes less reasonable as TCP diameter increases.

The time rate of change of thermal energy, q (W), stored by a section of the TCP may be represented by a heat balance equation:

$$[7] \quad q_{\text{net}} = q_{\text{in}} - q_{\text{out}} \\ = q_{\text{convection}} + q_{\text{incident radiation}} - q_{\text{emitted radiation}}$$

Each term on the right-hand side of this equation is a function of TCP temperature and other variables as described below. Heat loss by conduction away from the TCP tip can be significant if there is a longitudinal temperature gradient (Heitor and Moreira 1993), such as when only the tip is exposed to flame, but is not significant when most of the probe is heated to roughly the same temperature, as was assumed in the model.

The instantaneous rate of temperature change of a cylindrical TCP is related to the inward, or net, flow of heat as described by the equation:

$$[8] \quad \frac{dT_{\text{TCP}}}{dt} = \frac{2q(t)''_{\text{net}}}{\rho r C_p}$$

where T_{TCP} is the TCP's temperature, and the product of the TCP's radius, r (m), bulk density, ρ ($\text{kg}\cdot\text{m}^{-3}$), and specific heat, C_p ($\text{J}\cdot\text{kg}^{-1}\cdot\text{K}^{-1}$), may be thought of as heat per unit area of TCP surface per Kelvin. Net heat flux as a function of time is denoted by $q(t)''_{\text{net}}$ ($\text{W}\cdot\text{m}^{-2}$). Note that, as the radius of a cylindrical TCP decreases, its rate of temperature change increases in response to a given net heat flux.

Equation 8 is deceptively simple, because net heat flux is a function of several variables including TCP temperature at time t . However, if it is assumed that, for the most part, $q(t)''_{\text{net}}$ is proportional to the energy flux from fuel burning proximal to the TCP, then the rate of temperature change should correspond to the rate of fuel consumption, with the greatest rates occurring when the flame temperature and gas velocity at the TCP tip are peaking.

By the same assumption, total energy released by the fuel is proportional to total net heat flux, that is, net heat flux integrated over time. This is equivalent to TCP temperature integrated over time or a double integration of eq. 8. Assuming further that heat of combustion varies little within a set of fuels, time-integrated TCP temperature should correlate with total fuel consumption.

Heat transfer to a TCP by convection

Convective heat flux at a TCP surface is proportional to the temperature difference between the surface and surrounding gases: $q''_{\text{conv}} = h(T_{\text{gases}} - T_{\text{TCP}})$ ($\text{W}\cdot\text{m}^{-2}$), where the proportionality is determined by the coefficient of convection, h ($\text{W}\cdot\text{m}^{-2}\cdot\text{K}^{-1}$). The coefficient is in turn a function of the velocity and physical properties of gases flowing over the TCP surface and the shape and orientation of the TCP (Heitor and Moreira 1993).

According to Santoni et al. (2002), there are no engineering correlations for estimating the coefficient of convection of any geometric shape in the turbulent and reactive flow of wildland flames. However, engineering correlations are available for cylinders in cross flow (e.g., Incropera and DeWitt 2002) and in axial flow in nonflaming gases. Studying flow along the axis of a long cylinder, Buchlin (1998) found that, as the flow becomes even slightly abaxial, the cross-flow component rapidly dominates convective heat transfer; thus, a standard cross-flow correlation for a cylinder was used in the model to estimate the coefficient of convection, h ($\text{W}\cdot\text{m}^{-2}\cdot\text{K}^{-1}$) (adapted from Incropera and DeWitt 2002):

$$[9] \quad h = 0.683 \frac{k}{D} \left(\frac{sD}{\nu} \right)^{0.466} \text{Pr}^{0.333}$$

where D is the diameter of the cylinder ($D = 2r$) and k , ν , and s are, the thermal conductivity ($\text{W}\cdot\text{m}^{-1}\cdot\text{K}^{-1}$), kinematic viscosity ($\text{m}^2\cdot\text{s}^{-1}$), and speed ($\text{m}\cdot\text{s}^{-1}$) of gases flowing over the TCP, respectively. The dimensionless Prandtl number, Pr , may be taken as 0.7 for combustion gases (Quintiere 2006). Values of thermal conductivity and kinematic viscosity for air were used in the model. The expression in parentheses in eq. 9 is the Reynolds number of a cylinder in cross flow. The coefficient and exponent values in eq. 9 are used for Reynolds numbers ranging from 40 to 4000, which is an adequate range for the temperatures and flow velocities involved.

The values of k and ν vary with air temperature, but the ratio $k/\nu^{0.466}$ varies little (from 4.55 to only 4.7 in fractional units) over the range 273 K to 1300 K; thus, h is a function of flow speed for the most part. Using a mean value of the above ratio (~ 4.6), eq. 9 can be rewritten as

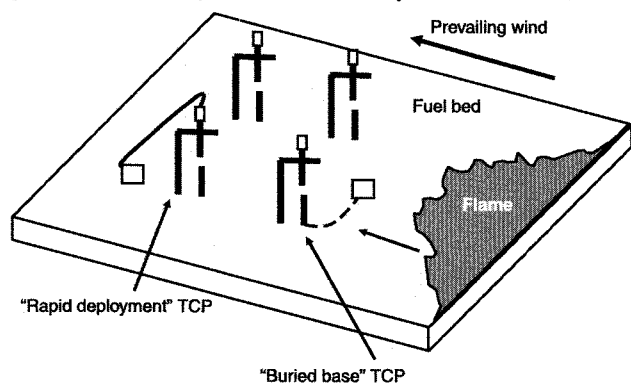
$$[10] \quad h \approx 2.8 \frac{s^{0.466}}{D^{0.534}}$$

where the value of $\text{Pr}^{0.333}$ is also contained in the coefficient. A correlation with values very close to those in eq. 10 may be found in Pitts et al. (1998).

Heat transfer to a TCP by radiation

An idealized model of thermal radiation from the flame is given by eqs. 4 and 5. Additional factors in radiative heating of a TCP include the absorbed (i.e., unreflected) proportion of incident thermal radiation, and the flame-to-probe view factor. The view factor (also called the shape or configuration factor) is the fraction of thermal radiation emitted by the flame wall that is intercepted by the TCP (Incropera and DeWitt 2002). It is a function of flame shape and physical dimensions, as well as distance from the TCP. In gen-

Fig. 2. Schematic of plot fire and TCP layout (not to scale).



eral, the view factor increases exponentially as a surface fire approaches a TCP.

Energy transferred to a TCP by thermal radiation, $q''_{\text{rad,in}}$ ($\text{W}\cdot\text{m}^{-2}$), was modeled using a relation similar to that in Wotton et al. (1999):

$$[11] \quad q''_{\text{rad,in}} = \bar{E} \frac{\alpha}{\pi} \int_{-L/2}^{L/2} \int_0^L \frac{d^2}{[d^2 + y^2 + (z - h_p)^2]^2} dz dy$$

where α is the mean absorptivity of 304 stainless steel, d (m) is the distance from the flame wall to the TCP, and h_p (m) is the height of the TCP tip above the fuel bed. Note that TCP orientation was not modeled, although it may influence the energy transferred by thermal radiation. Thermal radiation emitted by the TCP was estimated by the Stefan-Boltzmann law (see the Surface fire section).

The double integral expresses the view factor between a plane and a receiving differential element. Wotton et al.'s (1999) relation incorporated a height-dependent expression for emissive power (i.e., $E = E(z)$) in the integrand. However, to decrease processing time, a constant, mean emittance, \bar{E} , for the flame wall was calculated (eq. 5).

Methods

Field experiments

In the spring of 2006, a series of 12 small plot burns were conducted in the Vinton Furnace Experimental Forest (VFEF) in southern Ohio as part of an effort to develop infrared mapping techniques for fire behavior. Local wind speed, temperature, and relative humidity data were gathered at 1 s intervals at two onsite weather stations. All burns were recorded by video cameras mounted above and behind the plots. Thermocouple probe deployment is described below.

Two separate 8 m \times 8 m plots were constructed (Fig. 2). Fuelbeds of a range of loadings consisted of dried hardwood leaves and 1, 10, and 100 h branch material collected from January to March 2004 from several mixed-oak stands at the VFEF. Stands were dominated in basal area by white and red oaks (*Quercus* spp.) and also contained maple (*Acer* spp.), tulip-poplar (*Liriodendron tulipifera* L.), and black gum (*Nyssa sylvatica* Marsh.) along with other less common species. To increase fuel consumption, milled, kiln-dried softwood lumber (0.95 cm^2) was added to some plots.

Fuel was weighed separately by class (litter, branches,

and milled wood) and spread as evenly as possible over the plots to ensure homogeneity of fuel depth and composition. Small fuel samples of each class and size (i.e., litter; 1, 10, 100 h branches; and milled wood) were oven-dried to obtain estimates of fuel moisture on a dry-mass basis. Two concrete pads (40 cm \times 40 cm) were set flush with the mineral soil surface in each of the plots. Following each burn, remaining litter fuel was removed from the pads and weighed so that consumption could be estimated. Exceptions occurred in three of the burns, because much of the remaining litter blew off of the plot before it could be weighed. All branch and milled wood fuel was collected and weighed in bulk postburn. Woody fuel consumption was calculated from preburn and postburn loadings.

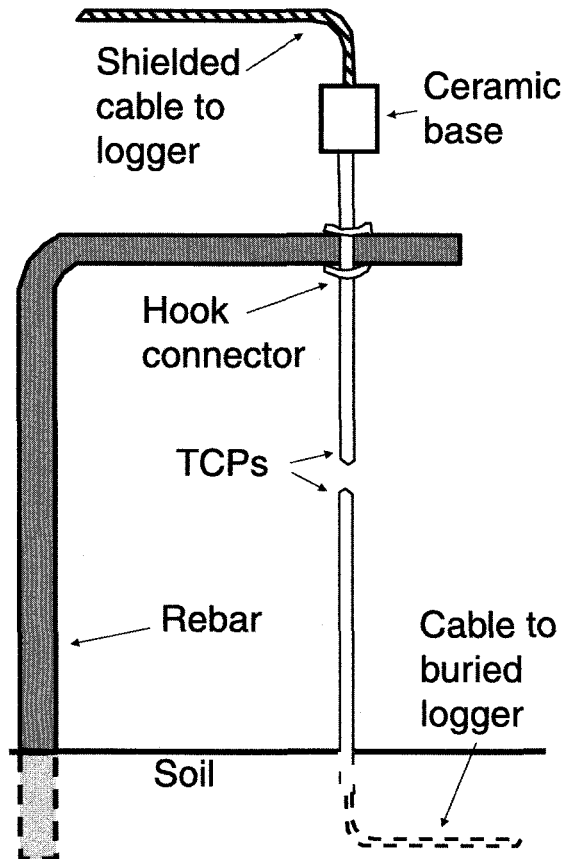
Four "high-temperature" stainless-steel TCPs (Onset Computer Corp., Bourne, Massachusetts) were erected vertically in the plots with their bases buried so that their tips were 25 cm above the mineral soil (Figs. 2 and 3). The TCP cables, also buried in soil, were connected to HOBO[®] type K thermocouple loggers (Onset Computer Corp., Bourne, Massachusetts, accuracy ± 14 $^{\circ}\text{C}$ at 625 $^{\circ}\text{C}$, maximum resolution 5 $^{\circ}\text{C}$). The loggers were then placed in PVC tubes buried so that their openings were nearly flush with soil. The tubes were capped and covered with concrete pads and then fuel. TCPs were placed at the corners of a 4 m \times 4 m square centered in the plot (Fig. 2).

In addition to the buried-base TCPs, four "rapid-deployment" TCP assemblies were tested in both plots (Figs. 2 and 3). These were designed to be mounted quickly within surface fire plots and to minimize soil and fuel disturbance. The TCPs used in this manner are identical in size and shape to the buried-base TCPs, but they have ceramic bases that can withstand exposure to flames. Each TCP was connected to a HOBO datalogger via a 2 m long Inconel[®]-wrapped, mineral-insulated thermocouple cable. The loggers were sandwiched between two 1.3 cm thick (10 cm wide \times 10 cm long) ceramic fiber boards (Cotronics Corp., Brooklyn, New York) that were wrapped on the outside with fire shelter material. The connected logger shelters were placed within the plot about 1 m from the TCP. In most trials, logger shelters were buried. However, in three burns, fuel was cleared from a small area (approximately 30 cm \times 30 cm) and a logger shelter was placed on the surface of the mineral soil in the center of the cleared area. All loggers placed in this manner were undamaged by the fires. The rapid-deployment TCPs were mounted, with the tip pointing down, on L-shaped rebar stakes by means of ring stand hook connectors. The tips were slightly above and within a 2 cm horizontal radius of the tips of the buried-base TCPs, forming four sets of pairs in each burn (Fig. 2).

Fires were started by drip torch on one edge of the plot (Fig. 2), except in two burns where, to mitigate the effect of a crosswind component, ignition lines were continued around the closest leeward corner to roughly midplot. This ensured that the resulting flame fronts were roughly perpendicular to the direction of spread by the time they reached the plot center.

Mean flame front velocities (i.e., rates of spread and directions) were estimated using the method of Simard et al. (1984) from the arrival times of flame fronts at the buried-base TCP tips. These rates of spread were used in calcula-

Fig. 3. Schematic diagram of "rapid-deployment" TCP.



tions of fire line intensity. Rates of fire spread, except in one burn, were also estimated from video.

Two types of flame residence time were estimated. Video recordings from the above-plot camera were used to obtain a mean of flame residence times estimated at three points in the fuel bed in each burn. Flame residence times at the TCP tips were estimated from the cumulative time over which the TCP's absolute rate of temperature change was greater than $2\text{ }^{\circ}\text{C}\cdot\text{s}^{-1}$. Although arbitrary, this threshold was chosen to filter out brief fluctuations in the rate, as shown in Fig. 4. The difference of estimated times from these two methods are reviewed in the discussion section.

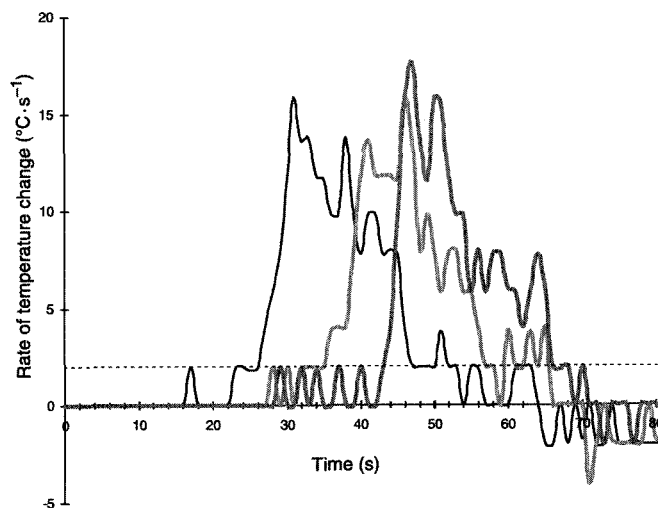
Maximum TCP temperature, T_{max} , was the greatest temperature recorded over the course of a burn. In keeping with past studies (e.g., Kennard et al. 2005), the area under the TCP temperature curve (A_{60}) was calculated by simple summation of all temperatures greater than or equal to $60\text{ }^{\circ}\text{C}$ multiplied by the time step (1 s). Time-integrated temperatures of paired buried-base and rapid-deployment TCPs were not significantly different ($p = 0.95$), so their values were averaged for each pair.

Mean wind speeds at the tips of the TCPs were estimated from wind speeds recorded at 2 m above the mineral soil according to a power law relation adapted from Mercer and Weber (1994): $\text{windspeed}_{\text{tip}} = \text{windspeed}_{2\text{ m}} \times [(0.25\text{ m} - \text{fuelheight}) / (2\text{ m} - \text{fuelheight})]^{0.143}$.

Implementation of the model

The TCP model was executed in Mathcad 2001i Profes-

Fig. 4. Rate of temperature change versus time for three separate TCPs in one plot fire. Flame contact was assumed to occur when the rate was $\geq 2\text{ }^{\circ}\text{C}\cdot\text{s}^{-1}$ (broken line).



sional (Parametric Technology Corporation, Needham, Massachusetts). To minimize processing time, eq. 11, which describes flame radiation transfer to a TCP, was approximated in the form of a double Riemann sum with spatial steps of 5 cm (i.e., $dy \approx \Delta y = 5\text{ cm}$, and $dz \approx \Delta z = 5\text{ cm}$). Over a range of parameter values, view factors generated by this approximation differed from those of the integral form by only $3.3\% \pm 0.014\%$ (mean \pm SD, $n = 28790$), but reduced the run time of the sensitivity tests (described below) from several hours to about 30 min on a 1.86 GHz Pentium M processor.

Flame residence times in the fuel bed and at the TCP tips were used in the simulations of plot burns. In the sensitivity and extended parameter tests, flame residence times in the fuelbed were estimated by dividing fuel consumption by a mean consumption rate of $0.04\text{ kg}\cdot\text{m}^{-2}\cdot\text{s}^{-1}$ (see Plot burns section). Flame base depths were then calculated by multiplying residence time by rate of spread.

Model sensitivity

To qualitatively illustrate the overall effects of parameters in the model, all combinations of five values of wind speed, consumed fuel loading, rate of spread, and mounting height ($n = 5^4 = 625$) were run for two TCPs of different diameters. Except for TCP height, the upper value of each parameter was chosen to reflect a relatively extreme condition (e.g., rate of spread of $0.3\text{ m}\cdot\text{s}^{-1}$) in a prescribed surface fire. Results of these runs are shown in Fig. 12. As described above, flame residence time in the fuel bed (and, accordingly, flame base depth) was a function of fuel consumption only. Therefore, flame residence times at modeled TCPs were dictated by TCP height and the model flame or plume profile (Fig. 1). The means of both TCP metrics (T_{max} and A_{60}) were calculated with respect to only the parameter (e.g., height) shown in any particular plot of Fig. 12. In other words, the SD (gray lines) of either metric is due to the combined effects of the remaining parameters. Therefore, the extent of the standard deviations is determined by the range of the remaining parameters.

Table 2. Thermocouple probe (TCP) metrics and fire characteristics of plot burns.

Burn	No. of working TCPs	Maximum TCP temperature (°C)*	Mean ambient temperature (°C)	Time-integrated temperature (A_{60} , °C)*	Residence time estimated from TCPs (s)*	Residence time estimated from raised camera (s)*	Mean rate of spread (m·s ⁻¹)	Mean wind speed at 2 m (m·s ⁻¹)	Fire line intensity (kW·m ⁻¹)
1	7	247±18	29	32 272 ± 5519	22.0±2.2	8.7±1.2	0.133	2.00	776
2	7	190±32	28	30 012 ± 7675	21.6±5.2	12.3±0.6	0.068	0.61	446
3	8	112±22	15	8022±2332	11.5±3.6	11.3±2.5	0.092	1.09	458
4	7	50±18	17	576±1090 [†]	2.0±1.4	7.7±1.5	0.058	1.39	144
5	8	145±14	16	8997±1513	17.0±1.9	6.3±6.3	0.101	2.02	504
6	7	157±77	19	28 140 ± 8761	18.6±19.5	16.0±5.2	0.013	0.51	196
7	8	285±77	22	64 104 ± 13 483	28.5±11.5	51.3±14.5	0.009	0.70	233
8	8	202±34	17	68 662 ± 21 230	16.1±9.5	64.0±31.2	0.006	0.48	201
9	8	166±48	24	19 898 ± 6026	16.0±5.1	13.3±3.8	0.043	0.46	407
10	8	90±16	25	7367±3241	5.1±3.6	8.7±5.7	0.023	0.63	116
11	7	426±25	31	148 256 ± 18 365	84.0±4.7	89.7±12.4	0.011	0.64	573
12	8	449±126	30	156 440 ± 27 398	80.5±10.9	73.7±17.6	0.013	0.45	698

*Values are means ± SDs.

[†]Six of eight TCPs had $A_{60} = 0$.

Table 3. Fuelbed measurements.

Burn	Litter loading (kg·m ⁻²)	Mean litter depth (cm)	Mean litter moisture (% dry mass)	Woody fuel loading (kg·m ⁻²)	Mean woody fuel depth (cm)	Mean woody moisture (% dry mass)	Total fuel loading (kg·m ⁻²)	Total dry loading (kg·m ⁻²)	Consumed dry loading (kg·m ⁻²)
1	0.70	8.3	7.6	—	—	—	0.70	0.65	0.36
2	0.70	8.3	8.7	1.6	18.9	21.7	2.26	1.93	0.41
3	0.35	4.9	12.4	—	—	—	0.35	0.31	0.31
4	0.17	2.3	11.7	—	—	—	0.17	0.16	0.16
5	0.35	4.4	12.4	—	—	—	0.35	0.31	0.31
6	0.70	7.8	11.4	1.6	15.1	23.4	2.30	1.93	0.93
7	1.05	13.5	13.6	1.6	14.5	27.4	2.65	2.18	1.57
8	0.70	8.1	10.2	2.5	13.8	15.4	3.20	2.80	2.12
9	0.70	7.7	7.6	—	—	—	0.70	0.65	0.59
10	0.35	4.4	7.3	—	—	—	0.35	0.33	0.31
11	1.05	10.4	10.3	2.5	14.2	13.0	3.54	3.15	3.15
12	1.05	10.4	9.7	2.8	18.7	13.8	3.87	3.43	3.36

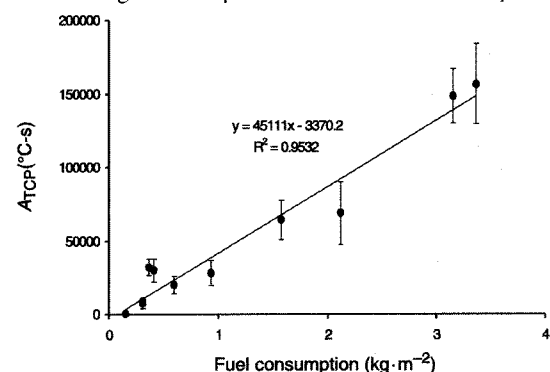
Other parameter values were varied singly to determine their effect. Separate plot fire simulations were run with TCP absorptivity values of 0.2, 0.3, and 0.4; time steps of 2, 1, 0.5, and 0.25 s; and heat of combustion values of 12 700, 16 000, and 18 700 kJ·kg⁻¹. Heat of combustion values were chosen to reflect the range in the literature (Johnson 1992).

Results

Plot burns

Rates of spread estimated from times of flame arrival at the TCPs (see Methods) agreed reasonably well with those estimated from overhead videos ($n = 11$, $R^2 = 0.90$, $SE = 0.012$ m·s⁻¹). Rates of spread were highly correlated with wind speed (Pearson $R \sim 0.8$, $P < 0.01$). TCP height above the soil surface was consistent across burns; however, because of differences in fuel loading, tip height above the top of the litter layer varied between 6 and 23 cm. Fire and TCP characteristics of the experimental burns, such as rates of spread and maximum TCP temperatures, are found in Table 2, while fuel loading, moisture and consumption are given in Table 3.

As expected, time-integrated temperature correlates best with consumed fuel loading (Fig. 5), which is, in turn, as-

Fig. 5. Time-integrated temperature versus fuel consumption.

sociated with flame residence time, both at the TCP tip and in the fuel bed. In fact, the ratio of fuel consumption to flame residence time within the fuel bed varied little: 0.04 ± 0.01 kg·m⁻²·s⁻¹ ($n = 12$).

Although time-integrated temperature diminished somewhat with wind speed, the effect was not significant at a 5% level in a multivariable regression. Regressing through zero and inverting the relation shown in Fig. 5, fuel consumption (kg·m⁻²) may be estimated from only time-integrated temperature by the following formula ($n = 12$, $SE = 0.27$ kg·m⁻²):

Fig. 6. Maximum excess temperature ($T_{TCP} - T_o$) versus fuel consumption.

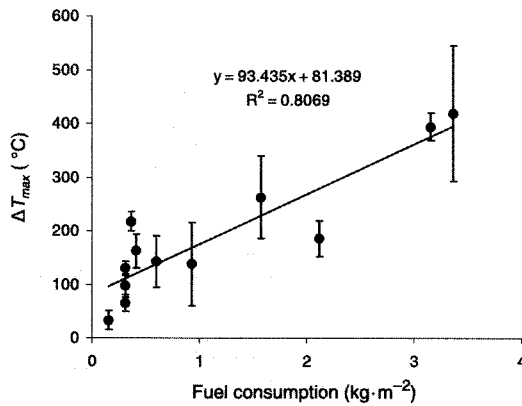
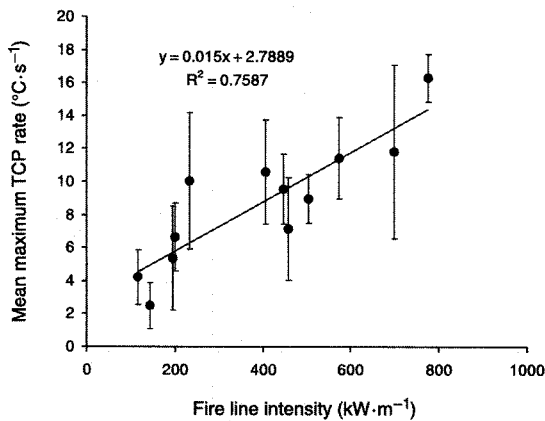


Fig. 7. The effect of fire line intensity on TCP rate of temperature change.



$$[12] \quad W_{\text{consumed}} = 2.23 \times 10^{-5} A_{TCP}$$

Maximum TCP temperature characterizes the integration of net heat flux, at least to the point of flame departure (Fig. 6). Inverting the relation shown in Fig. 6, fuel consumption may be roughly estimated from maximum TCP temperature using

$$[13] \quad W_{\text{consumed}} = 0.007 \Delta T_{\text{max}}$$

($n = 12$, $SE = 0.57 \text{ kg}\cdot\text{m}^{-2}$), where $\Delta T_{\text{max}} = T_{\text{max}} - T_o$ is maximum excess TCP temperature.

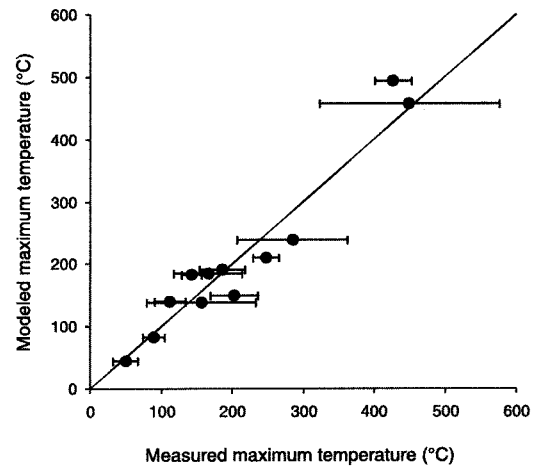
Mean maximum rates of temperature change increased with increasing fire line intensity. Inverting the relation shown in Fig. 7, fire line intensity may be estimated from maximum TCP rate by

$$[14] \quad I = 46 \left. \frac{dT}{dt} \right|_{\text{max}}$$

($n = 12$, $SE = 110 \text{ kW}\cdot\text{m}^{-1}$).

Equations 12, 13, and 14 were generated by regression through the origin, because the constants of all three linear equations were not significant in ordinary least squares regressions. This is also reasonable from a physical standpoint; absence of fire should result in ΔT , A_{60} , and dT/dt values of zero. Coefficients of determination have not been

Fig. 8. Modeled versus measured maximum TCP temperatures. The diagonal line represents one-to-one correspondence.



included in the above statistics, because their meaning is unclear in regressions through the origin (Eisenhauer 2003).

Simulations of TCPs in plot burns

Using values of rate of spread, estimated flame residence times in the fuel bed (see Methods section), consumed fuel loading, TCP tip height, and mean wind speed from the small-plot experiments (Tables 2 and 3), the model generated only adequate estimates of maximum TCP temperature ($R^2 = 0.75$, $SE = 78 \text{ }^\circ\text{C}$). However, estimates of time-integrated temperature were much closer to measured values ($R^2 = 0.93$, $SE = 13.8 \times 10^4 \text{ }^\circ\text{C}\cdot\text{s}$).

Estimates of maximum temperature improved significantly when model flame dimensions were adjusted so that flame residence times matched those at the TCP tips, rather than in the fuel bed (Fig. 8). Standard error of estimate was halved ($SE = 37 \text{ }^\circ\text{C}$), and the correlation coefficient between residence time and measured maximum temperatures increased to $R^2 = 0.93$. The correlation to measured values remained the same for estimates of time-integrated temperature ($R^2 = 0.93$), and the SE dropped slightly to $13.4 \times 10^4 \text{ }^\circ\text{C}\cdot\text{s}$ (Fig. 9).

Modeled maximum rates of temperature change did not correlate well with measured rates ($R^2 < 0.10$) and were overestimated by a mean of $8 \text{ }^\circ\text{C}\cdot\text{s}^{-1}$, regardless of flame residence times (Fig. 10). In the model, rate maxima occurred during exposure to maximum flame temperature (i.e., when the flame center passed over the TCP). This is in contrast to experimental cases, where the maximum rate usually occurs not long after initial flame contact.

As an example of model output, Fig. 11 compares modeled TCP temperature plotted with TCP responses to a burn. Temperature profiles from TCPs in burn 2 were aligned so that peak temperatures occurred at the same time. Mean temperature and SD were then calculated for each time step (shaded broken line and shaded area, respectively). Note the considerable variation in maximum TCP temperatures that occurred over a relatively small spatial scale ($\sim 4 \text{ m}$) in a plot that was uniformly loaded with fuel.

Model sensitivity

The effects of varying model parameters are illustrated

Fig. 9. Modeled versus measured maximum time-integrated temperatures. The diagonal line represents one-to-one correspondence.

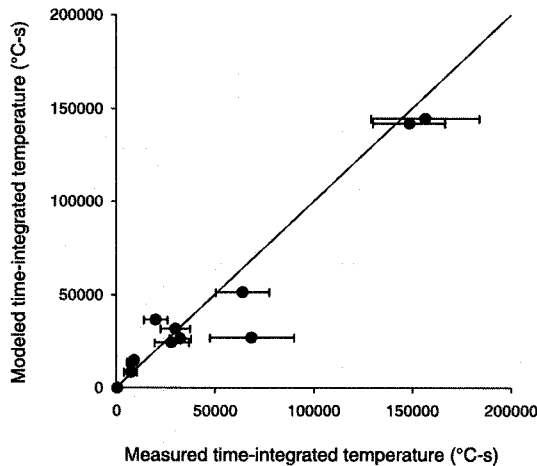
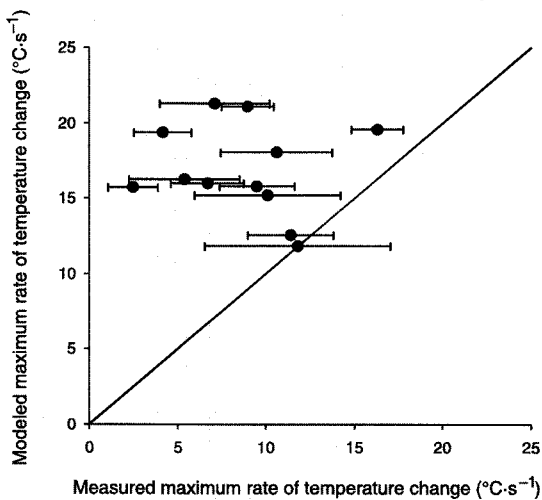


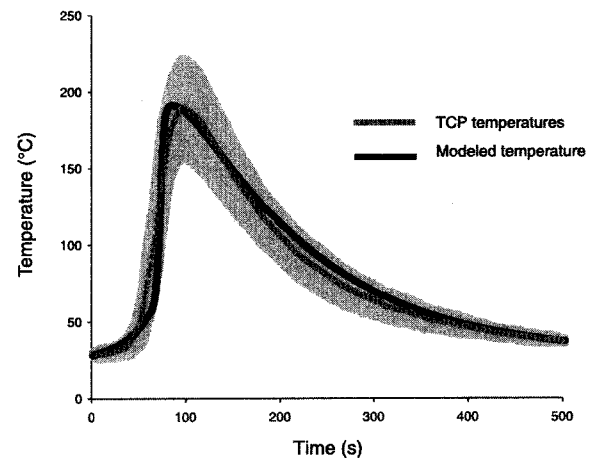
Fig. 10. Modeled versus measured maximum rates of temperature change. The diagonal line represents one-to-one correspondence.



in Fig. 12. Notice that, for any given parameter value, there is a wide range of possible maximum or time-integrated temperatures, owing to variation in the other parameters. This is especially true for TCP height and wind speed. Although it is apparent that modeled time-integrated temperature in particular diminishes as these parameters increase, variation in the other parameters—most likely fuel consumption—generates a wide range in the SD. A caveat is that the flame and plume model is primitive (Fig. 1), so we would expect these plots to change somewhat if a more sophisticated flame model was employed.

From Fig. 12, it is clear that TCP diameter has a greater effect on maximum temperature than on time-integrated temperature. This is because TCPs of a smaller diameter have a higher surface area/volume ratio (proportional to the $1/r$ term in eq. 8) and will attain higher temperatures than TCPs of larger diameter given the same heat flux. Although this may increase time-integrated temperature prior to flame departure, smaller diameter TCPs will also lose energy more rapidly afterward; thus, there is only a modest effect on time-integrated temperature overall. Of all

Fig. 11. Simulation of TCP temperature in a plot fire. Model output (black line) is plotted on top of the mean of measured TCP temperatures (shaded broken line) and standard deviation (shaded area).



the parameters, Fig. 12 indicates that consumed fuel loading had the strongest effect on maximum and time-integrated temperature.

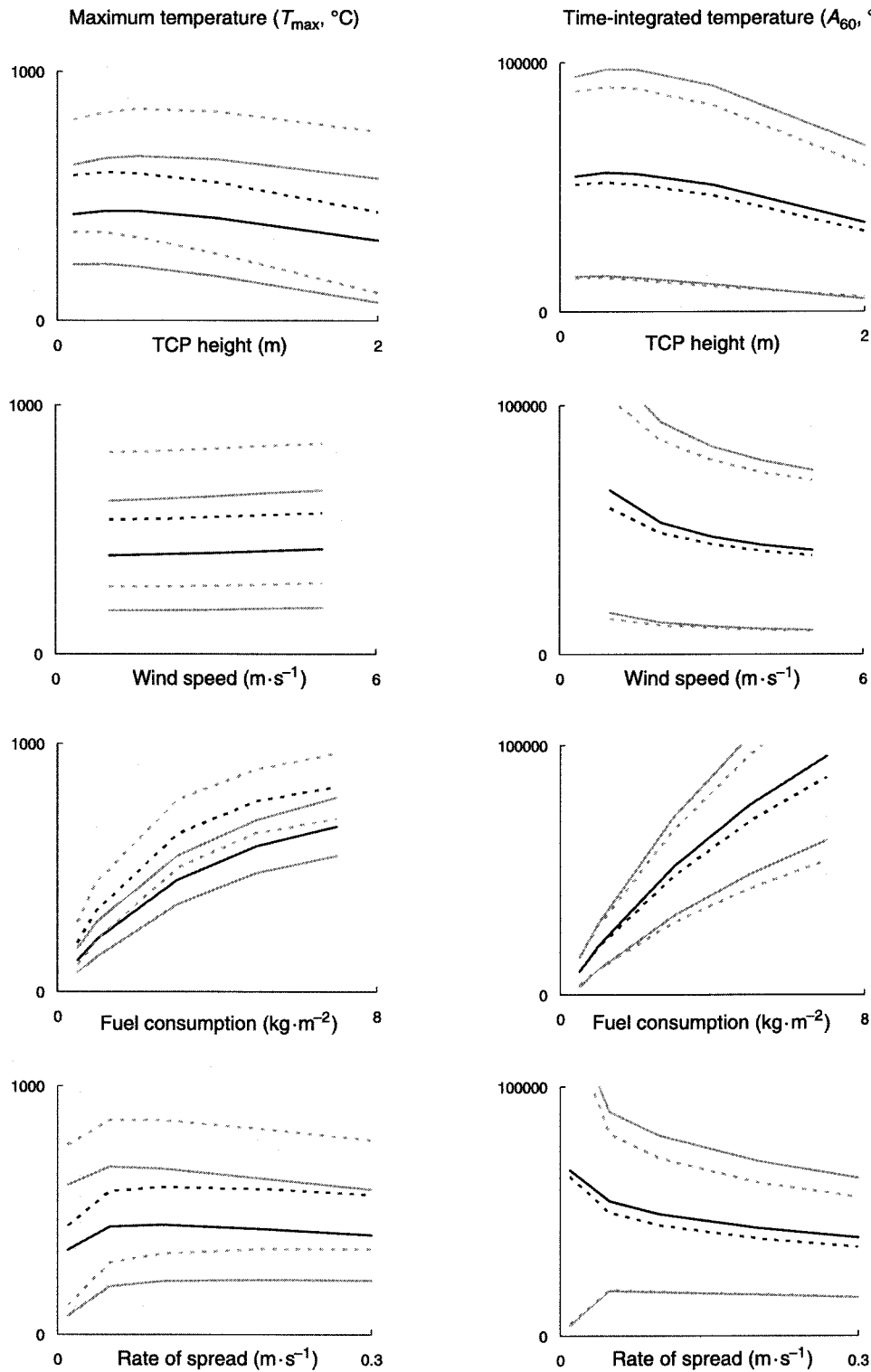
In the simulations, maximum TCP temperatures modeled using the highest heat of combustion were 0.9% higher, on average, than those at the lowest. The mean value of time-integrated temperatures increased by only 4.8% over the same range. Both maximum and time-integrated temperatures were relatively insensitive to changes in time step. The means of modeled maximum and time-integrated TCP temperatures decayed as Δt^2 and decreased by only 0.5% and 0.2%, respectively, between time steps of 1 and 0.5 s. Absorptivity (α) proved to be a critical parameter in model output. Increasing its value from 0.2 (the value chosen for the simulations) to 0.3 increased the means of maximum and time-integrated TCP temperatures by 12% and 29%, respectively, and decreased the accuracy of the simulations.

Discussion

Results from the experimental plot burns suggest that good estimates of total dry fuel consumption in surface fires may be made from the summed temperature of TCPs (eq. 12). If temperature–time profiles are not available, then maximum TCP temperature may be used to estimate consumption, although with a larger margin of error (eq. 13). Using bare thermocouples in grassland fires, Stronach and McNaughton (1989) reported significant ($p < 0.001$) but much weaker correlations between consumed fuel loading and summed temperature ($R^2 = 0.57$) and maximum temperature ($R^2 = 0.53$). However, their thermocouples were mounted within a grass fuel canopy, over heights ranging from 2 to 72 cm, and all measurements were combined, which may have weakened the correlations.

Other factors aside, it is, of course, the energy released by flaming and, to a lesser extent, smoldering combustion that determine the area under the temperature–time curve of TCPs exposed to surface fires. However, heat of combustion is usually regarded as a constant in wildland fires and is not the primary factor in surface fire intensity (Johnson 1992), so it is reasonable in this case to regard the quantity of con-

Fig. 12. Effects of model parameters on maximum TCP temperature (T_{max}) (left column) and time-integrated TCP temperature (A_{60}) (right column). Lines are mean values (black lines) and ± 1 SD (shaded lines) of 4.8 mm (solid lines) and 2.4 mm (broken lines) diameter TCPs.



sumed dry fuel as a surrogate of total energy released. This was also suggested in sensitivity tests of the model, because varying the heat of combustion had little effect on the modeled metrics.

Data from the plot burns also indicate that one may be able to use TCPs to obtain rough estimates of fire line inten-

sity from maximum rates of temperature change (eq. 14), especially in larger fires. Separate estimates of fire line intensity may be made by combining estimates of fuel consumption from time-integrated TCP temperature (eq. 12) with rates of spread estimated using the method of Simard et al. (1984) (see Methods). Intensities estimated by these

different methods could then be averaged. As might be expected from the theme of this paper, eqs. 12–14 are applicable when only the same type of TCPs that were used in these experiments (see TCP thermophysical properties section) are deployed in a manner similar to that described above (see Methods section).

The differences between flame residence times in the fuel bed and at the TCP tip ranged from 1 to 48 s. The disparities resulted because TCP tips were exposed to flames for different lengths of time than flames were present in the fuel bed, most likely because of small flame size, flickering, and changes in wind direction. Flame contact (i.e., convective heating) with a TCP's tip generally has a greater effect on its rate of temperature change than does radiation alone. TCP tip heights above the fuel surface ranged from about 22 cm to as little as 6 cm in the experiments above. This suggests that, to obtain accurate fuel bed residence times, TCP tips should be placed at or just above the fuel surface so that flame contact is assured.

Because of the prescribed triangular flame, the modeled residence time of the flame at the TCP is determined solely by tip height and the depth of the flame base. This is a crude approximation of a parameter that is influenced by several factors, especially changes in wind velocity. Not surprisingly, flame residence time at the TCP tip is a key factor in TCP response to fire. This is confirmed by the significant improvement in correlation between modeled and measured TCP metrics when estimated flame residence times at the TCPs tips were substituted for those at the fuel surface. A more advanced flame model will give better estimates of flame residence times, although at the expense of increased processor time.

In the model, the wind speed parameter affects resultant gas velocity and the coefficient of convection (eq. 10) but does not modify flame shape. A model incorporating flame tilt would likely show an increased influence of wind on TCP metrics, at least for TCPs mounted high above the fuel bed where tilted flames might not make contact.

Validation of the model is incomplete, because TCPs of only one diameter were deployed over a limited range of relatively low tip heights above the fuel bed. However, for the available data, the agreement between measured and modeled TCP metrics, with the exception of rate of temperature change, is surprisingly good, especially considering the simplicity of the flame model.

For TCPs in surface fires, maximum rates seem to occur almost as soon as flames make contact. Obviously, this is not captured in the model (Fig. 10). This is likely due to a combination of factors. For instance, the highly idealized model flame, unlike a true surface fire flame, exposes the modeled TCP to a continuous and monotonically rising gas temperature during the first half of contact. Also, TCPs in the model are always exposed to the highest possible flame temperature, which is probably unlikely in the highly varying environment of a surface fire flame.

Estimating rates of temperature change in the actual TCPs was complicated by the relatively low temperature resolution of the dataloggers (see Methods section), which causes a "stepped" response and so limits the possible rates (Fig. 4). However, temperature rate is perhaps the least useful of TCP metrics, because it seems to provide only rough

estimates of fire line intensity (eq. 14). Furthermore, TCPs of smaller diameter will give higher (eq. 8), and most likely less distinguishable, rates regardless of intensity.

The success of the model in simulating TCP response to surface fire suggests that using a TCP model to make inverse estimates of fire characteristics may be possible. Inverse estimates are, roughly speaking, those in which causes are estimated from effects. As an example, various fuel consumptions and rates of spread could be tested until a close match is found to an actual temperature–time curve of a TCP in a surface fire. Such estimates would undoubtedly be improved by the inclusion of a more advanced flame model, although this would necessarily increase processor time. However, nonlinearities in a model and nonuniqueness of results (for instance, the same fire line intensity can be calculated for any combination of consumed loading and rate of spread satisfying the relation $WRh_c = \text{constant}$) greatly complicate the inverse process. Given the multivariate dependence of TCP response to fire, it is not certain that an inverse approach will be fruitful.

The rapid-deployment TCP sets (Figs. 2 and 3) performed well and were undamaged in the plot fires. In most cases, sheltered loggers were buried in a shallow hole in the soil. However, due to prolonged heating of the soil, especially in cases of high fuel loading, the better approach may be to place the sheltered loggers on the soil surface in a small area ($\sim 30 \text{ cm} \times 30 \text{ cm}$) from which fuel has been cleared. Clearing away surface fuel is necessary because, although fire shelter material is highly reflective of radiant energy, it provides little protection from convective heating, especially during direct flame contact.

Because they are economical and easy to deploy, it is likely that TCPs will continue to be used in prescribed surface fires. However, as monitoring and remote sensing technologies progress, devices that measure the heat release of surface fires more directly will become less expensive and probably preferable to devices such as TCPs that integrate both convective and radiant heating from flames. For example, data from small infrared sensors deployed in prescribed burns, and in the experiments described above, correlated better with consumed fuel loading (unpublished data). Infrared sensors have the added advantage of integrating over a variable field of view unlike TCPs which respond to only local conditions.

Conclusions

Reporting device temperatures is not a useful way to compare studies of wildland fires, because device temperatures are not mechanistically related to the behavior of fires or their effects; just as important, the types of devices and their deployments are rarely consistent among studies. We have shown that, in principle, TCP response to wildland fires can be modeled and, therefore, that it may be possible to inversely estimate certain fire characteristics from uncalibrated TCP data. Over combinations of a wide range of parameters, model results suggest that fuel consumption has the greatest effect on TCP response. As well, TCP data can be used to estimate some fire characteristics directly using calibration relationships.

Thermocouple probes are not a panacea for fire monitoring. Given that their response is primarily driven by convec-

tive heating within the flame and short-range radiative heating, they are largely point estimates of fire and fuel bed characteristics. Thus, one can expect estimates of fire characteristics derived from TCPs to be highly variable spatially. As well, calibration relationships must span the range in fire characteristics and, until more data are available, must be assumed to be valid only within a given fuel type. In addition, we recommend that thermocouple probes be positioned in the flame at a consistent height above the fuelbed (not the soil surface). Finally, TCPs reflect fuel consumption and flame residence time, yet are not as accurate in describing fire line intensity. Accordingly, having independent estimates of flame rate of spread is helpful for estimating fire line intensity directly.

Acknowledgments

Thanks to Bill Borovicka, David Hosack, Jimmy Stockwell, Brad Tucker, and Kristy Tucker of the VFEF for field assistance. Funding for this project came from the Central Hardwoods National Fire Plan project.

References

- Archibold, O.W., Nelson, L.J., Ripley, E.A., and Delaney, L. 1998. Fire temperatures in plant communities of the northern mixed prairie. *Can. Field-Nat.* **112**: 234–240.
- Bailey, A.W., and Anderson, M.L. 1980. Fire temperatures in grass, shrub and aspen communities of central Alberta. *J. Range Manage.* **33**: 37–40. doi:10.2307/3898225.
- Bauer, W., Oertel, H., and Rink, M. 2003. Spectral emissivities of bright and oxidized metals at high temperatures. Presented at the 15th Symposium on Thermophysical Properties, 22–27 June 2003, Boulder, Colo. Available from symp15.nist.gov/pdf/p.682.pdf.
- Briz, S., de Castro, A.J., Aranda, J.M., Mendelez, J., and Lopez, F. 2003. Reduction of false alarm rate in automatic forest fire infrared surveillance systems. *Remote Sens. Environ.* **86**: 19–29. doi:10.1016/S0034-4257(03)00064-6.
- Buchlin, J.-M. 1998. Natural and forced convective heat transfer on slender cylinders. *Rev. Gen. Thermique*, **37**: 653–660. doi:10.1016/S0035-3159(98)80043-3.
- Butler, B.W., Cohen, J., Latham, D.J., Schuette, R.D., Sopko, P., Shannon, K.S., Jimenez, D., and Bradshaw, L.S. 2004. Measurements of radiant emissive power and temperatures in crown fires. *Can. J. For. Res.* **34**: 1577–1587. doi:10.1139/x04-060.
- Buttsworth, D.R. 2001. Assessment of effective thermal product of surface junction thermocouples on millisecond and microsecond time scales. *Exp. Thermal Fluid Sci.* **25**: 409–420. doi:10.1016/S0894-1777(01)00093-0.
- Dickinson, M.B., and Johnson, E.A. 2001. Fire effects on trees. *In* Forest fires: behavior and ecological effects. Edited by E.A. Johnson and K. Miyanishi. Academic Press, New York. pp. 477–525.
- Drysdale, D. 1998. An introduction to fire dynamics. John Wiley Sons, Ltd., West Sussex, England. pp. 48–52.
- Dupuy, J.L., Marechal, J., and Morvan, D. 2003. Fire from a cylindrical forest fuel burner: combustion dynamics and flame properties. *Combust. Flame*, **135**: 65–76. doi:10.1016/S0010-2180(03)00147-0.
- Eisenhauer, J.G. 2003. Regression through the origin. *Teach. Stat.* **25**: 76–80. doi:10.1111/1467-9639.00136.
- Gardner, L., and Ng, K.T. 2006. Temperature development in structural stainless steel sections exposed to fire. *Fire Saf. J.* **41**: 185–203. doi:10.1016/j.firesaf.2005.11.009.
- Heitor, M.V., and Moreira, L.N. 1993. Thermocouples and sample probes for combustion studies. *Prog. Energy Combust. Sci.* **19**: 259–278. doi:10.1016/0360-1285(93)90017-9.
- Incropera, F.P., and DeWitt, D.P. 2002. An introduction to heat transfer. 4th ed. John Wiley Sons, Inc., New York. pp. 240–245.
- Iverson, L.R., Yaussy, D.A., Rebeck, J., Hutchinson, T.L., Prasad, R., and Long, A.M. 2004. A comparison of thermocouples and temperature paints to monitor spatial and temporal characteristics of landscape-scale prescribed fires. *Int. J. Wildland Fire*, **13**: 311–322. doi:10.1071/WF03063.
- Johnson, E.A. 1992. Fire and vegetation dynamics. 1st ed. Cambridge University Press, New York. pp. 40–43.
- Karlsson, B., and Ribbing, C.G. 1982. Optical constants and spectral selectivity of stainless steel and its oxides. *J. Appl. Phys.* **53**: 6340–6346. doi:10.1063/1.331503.
- Kennard, D.K., Outcalt, K.W., Jones, D., and O'Brien, J.J. 2005. Comparing techniques for estimating flame temperature of prescribed fires. *Fire Ecol.* **1**: 75–84.
- Lippincott, C.L. 2000. Effects of *Imperata cylindrica* (L.) Beauv. (cogongrass) invasion on fire regime in Florida Sandhill (USA). *Nat. Areas J.* **20**: 140–149.
- McCaffrey, B.J. 1979. Purely buoyant diffusion flames: some experimental results. Center for Fire Research, National Bureau of Standards, Gaithersburg, Md. NBSIR 79-1910.
- Mercer, G.N., and Weber, R.O. 1994. Plumes above line fires in a cross wind. *Int. J. Wildland Fire*, **4**: 201–207. doi:10.1071/WF9940201.
- Nelson, R.M., Jr. 2002. An effective wind speed for models of fire spread. *Int. J. Wildland Fire*, **11**: 153–161. doi:10.1071/WF02031.
- Otsuka, A., Hosono, K., Tanaka, R., Kitagawa, K., and Arai, N. 2005. A survey of hemispherical total emissivity of the refractory metals in practical use. *Energy*, **30**: 535–543. doi:10.1016/j.energy.2004.04.019.
- Paloposki, T., and Liedquist, L. 2005. Steel emissivity at high temperatures. VTT Technical Research Centre of Finland, Oulu, Finland. VTT Tiedotteita Res. Notes, 2299. Available from www.vtt.fi/inf/pdf/. [Accessed 22 May 2007.]
- Pastor, E., Rigueiro, A., Zarate, L., Gimenez, A., Arnaldos, J., and Planas, E. 2002. Experimental methodology for characterizing flame emissivity of small scale forest fires using infrared thermography techniques. *In* Forest fire research and wildland fire safety. Edited by D.X. Viegas. Millpress, Rotterdam, the Netherlands.
- Pitts, W.M., Braun, E., Peacock, R.D., Mitler, H.E., Johnsson, E.L., Reneke, P.A., and Blevins, L.G. 1998. Temperature uncertainties for bare-bead and aspirated thermocouple measurements in fire environments. Presented at the 14th Meeting of the United States – Japan Conference on the Development of Natural Resources (UJNR) Panel on Fire Research and Safety, 28 May – 3 June 1998, Tsukuba, Japan. *In* Thermal Measurements: The Foundation of Fire Standards. ASTM STP 1427. Edited by L.A. Grizo and N.J. Alvares. American Society for Testing and Materials, West Conshohocken, Pa.
- Quintiere, J.G. 2006. Fundamentals of fire phenomena. 1st ed. John Wiley Sons Ltd., West Sussex, England. pp. 15–16.
- Santoni, P.-A., Thierry, M., and Leoni, E. 2002. Measurement of fluctuating temperatures in a continuous flame spreading across a fuel bed using a double thermocouple probe. *Combust. Flame*, **131**: 47–58. doi:10.1016/S0010-2180(02)00391-7.
- Simard, A.J., Eenigenburg, J.E., Adams, K.B., Nissen, R.L., and Deacon, A.G. 1984. A general procedure for sampling and analyzing wildland fire spread. *For. Sci.* **30**: 51–64.
- Stronach, N.R.H., and McNaughton, S.J. 1989. Grassland fire dy-

- namics in the Serengeti ecosystem, and a potential method of retrospectively estimating fire energy. *J. Appl. Ecol.* **26**: 1025–1033. doi:10.2307/2403709.
- Van Wagner, C.E., and Methven, I.R. 1978. Discussion: two recent articles on fire ecology. *Can. J. For. Res.* **8**: 491–492. doi:10.1139/x78-075.
- Victor, A.C., and Douglas, T.B. 1960. Physical properties of high temperature materials. Part VI. Enthalpy and heat capacity of magnesium oxide, zirconium oxide and zirconium silicate from 0 to 900 °C. National Bureau of Standards, Washington, D.C. Rep. WADC-TR-57-374(pt. VI).
- Walker, J.D., and Stocks, B.J. 1968. Thermocouple errors in forest fire research. *Fire Technol.* **4**: 59–62. doi:10.1007/BF02588607.
- Wally, A.L., Menges, E.S., and Weekley, C.W. 2006. Comparison of three devices for estimating fire temperatures in ecological studies. *Appl. Veg. Sci.* **9**: 97–108. doi:10.1658/1402-2001(2006)9[97:COTDFE]2.0.CO;2.
- Williamson, G.B., and Black, E.M. 1981. High temperatures of forest fires under pines as a selective advantage over oaks. *Nature (London)*, **293**: 643–644. doi:10.1038/293643a0.
- Wotton, B.M., McAlpine, R.S., and Hobbs, M.W. 1999. The effect of fire front width on surface fire behaviour. *Int. J. Wildland Fire*, **9**: 247–253. doi:10.1071/WF00021.
- Yuan, L.-M., and Cox, G. 1996. An experimental study of some line fires. *Fire Saf. J.* **27**: 123–129. doi:10.1016/S0379-7112(96)00047-1.